Available online at www.sciencedirect.com
ScienceDirect
Journal of Power Sources 162 (2006) 773–779
JOURNAL OF POWER SOURCES
www.elsevier.com/locate/jpowsour

Advanced manganese oxide material for rechargeable lithium cells

Terrill B. Atwater[a,b,*], Alvin J. Salkind[a,c]

[a] *Rutgers University, Piscataway, NJ, USA*
[b] *US Army RDECOM, CERDEC, Ft. Monmouth, NJ 07703, USA*
[c] *Robert Wood Johnson Medical School, New Brunswick, NJ, USA*

Received 8 February 2005
Available online 10 January 2006

Abstract

A family of potassium-doped manganese oxide materials were synthesized with the stoichiometric formula $Li_{0.9-X}K_XMn_2O_4$, where $X = 0.0$–0.25 and evaluated for their viability as a cathode material for a rechargeable lithium battery. A performance maximum was found at $X = 0.1$ where the initial specific capacity for the lithium–potassium-doped manganese dioxide electrochemical couple was 130 mAh g^{-1} of active cathode material. The discharge capacity of the system was maintained through 90 cycles (95% initial capacity). Additionally, the capacity was maintained at greater than 90% initial discharge through 200 cycles. Other variants demonstrated greater than 75% initial discharge through 200 cycles at comparable capacity.

Keyword: Rechargeable lithium cells

1. Introduction

Batteries are typically the limiting factor in the performance of most commercial and military portable electronic equipment. This is due to the restrictions on the size, weight and configuration placed by the equipment on the power source. Lithium polymer electrolyte batteries with their high energy density, conformal packaging and improved safety are one of the most promising electrochemical systems under development today.

Manganese dioxide-doped with potassium was examined as a cathode material for rechargeable lithium and lithium-ion batteries. The goal of this effort was to provide a new mixed metal oxide cathode material for use as the positive electrode in rechargeable lithium and lithium-ion electrochemical cells. A stable mixed metal oxide was fabricated by doping manganese dioxide with potassium. This material was then used as an intermediate for further processing and lithiation for use in rechargeable lithium batteries [1].

Electrochemical measurements were performed on rechargeable lithium batteries using potassium-doped manganese dioxide as the positive electrode. The changes in cell behavior as a function of potassium stoichiometry in MnO_2 were evaluated. Optimization of cell discharge and charge properties with respect to the potassium and lithium stoichiometry was a goal during these measurements. Additional research was focused on the characterization of the $Li_{0.9-X}K_XMn_2O_4$ material and the stability of cell components. For comparison $Li//Li_{0.9}Mn_2O_4$ electrochemical cells were fabricated and evaluated in parallel with the $Li//Li_{0.9-X}K_XMn_2O_4$ electrochemical cells.

2. Background

Manganese dioxide (MnO_2) is used as the base material in many active cathodes for rechargeable lithium batteries. MnO_2 is attractive because of its high energy density and low material cost. Manganese dioxide (MnO_2) serves as a skeletal background for lithium intercalation during cycling of a rechargeable cell. The cathode of a fully charged

* Corresponding author. Tel.: +1 732 427 3549; fax: +1 732 427 3665.
E-mail address: Terrill.B.Atwater@us.army.mil (T.B. Atwater).

0378-7753/$ – see front matter © 2005 Elsevier B.V. All rights reserved.
doi:10.1016/j.jpowsour.2005.07.048

lithium/MnO_2 cell is simply a continuous skeletal lattice structure of various MnO_2 crystal structures. When fully charged, manganese particles have a meta-stable 4+ valence state. This meta-stable 4+ valence state allows for the attraction and intercalation of lithium cations into the lattice structure. As lithium cations fill, the skeleton crystal structure during discharge, the crystal structure of the material changes. Charging of the cell removes these lithium cations from the cathode, again altering the crystal structure. Ideally, this is a completely efficient and reversible process, but realistically these continuous phase transitions lead to performance degradation. The frequent charge/discharge of a battery cell through cycling results in unwanted phase transitions of the crystal structure. Unwanted crystal structures develop that are either too stable for electrochemical reactions or block the insertion/extraction paths of lithium cations into the cathode material. This general phenomenon is regarded as one of the largest contributors to cathodic capacity fading [2–15].

Capacity fading of the cathode, a major cause of performance degradation, has been linked to fracture of active material. Fracture is caused by mechanical strain of MnO_2 crystal structures during cycling of the cell. Strain of crystal structures is related to phase transitions. The cathode crystal structure changes as more lithium incorporates into the cathode skeleton, the crystals increase in size and alter in shape. This frequent conversion in geometry and dimension of the crystal lattice create a significant mechanical strain on the cathode. This mechanical strain is believed to electrically disconnect active material from the electrode through fracture. Elevated temperatures also promote cathode fracture; structural vibrations increase with temperature, resulting in disconnection. Electrically disconnected active material is believed to block pathways for lithium cation insertion/extraction, causing the inactivation of more MnO_2 particles [2–4,7,12].

Cathode fracture is caused mostly by structural disorder of the MnO_2 crystals, and strain energy of the overall material. Through cycling, large particles have been known to split into multiple smaller particles. This splitting mechanism is related to the strain and surface energies of the particles. Once the increase in strain energy has reached a certain threshold, new surfaces are formed on the particles, causing them to split. Some of the small particles become disconnected from the binder, dissolving into the electrolyte. Once dissolved into the electrolyte, some of these smaller particles block lithium cation insertion/extraction pathways, deactivating more MnO_2 particles [4,12,13].

Usually, strain related fracture occurs during discharge. The mechanical stability of a fully charged Mn^{4+} skeleton is reduced with discharge. Also, insertion of lithium cations into the skeleton structure increases strain. As lithium cations are inserted and extracted, the bulk cathode expands and contracts, respectively. A 16% increase in strain has been measured in MnO_2 cathode structures [9]. The volume also increases along with cubic to tetragonal phase transitions. Defects in the cathode material may be beneficial in limiting this mechanism. Inactive material (Mn_2O_3 and Mn_3O_4) is known to retain their crystal structure through discharge and lessen dimensional changes of the matrix. This reduces the mechanical strain of the bulk cathode material. Incorporation of inactive Mn_2O_3 and Mn_3O_4 may lower the efficiency of the cathode, but it will strengthen its mechanical properties [4,7,13].

Capacity fading is the loss of cycle capacity in a cell over the entire life of a battery system, limiting the practical number of cycles that may be used. In lithium battery systems, capacity loss is attributed to the degradation of the active cathode material. This degradation is a result of phenomena that occurs during the charging and discharging of the cell. It is a result of both changes in composition and crystal structure of the active material. Also throughout the life of a cell, parasitic side reactions occur between the chemical species of all cell components; these reactions include chemical dissolution and degradation of the active cathode material. Methods of reducing this effect include changing the crystal structure and/or composition of the active material [1–3,12,14].

Manganese dioxide-doped with potassium was examined as a cathode material for rechargeable lithium and lithium-ion batteries. The goal of this effort was to provide a new mixed metal oxide cathode material for use as the positive electrode in rechargeable lithium and lithium-ion electrochemical cells. A stable mixed metal oxide was fabricated by doping manganese dioxide with potassium. This material was then used as an intermediate for further processing and lithiation for use in rechargeable lithium batteries [1].

3. Experimental

The $Li_{0.9-X}K_XMn_2O_4$ material used in this study was prepared through a series of solid-state reactions. Mixing KOH and MnO_2 and heating in an annealing oven for 72 h resulting in $K_XMn_2O_4$. The material was further processed forming $Li_{0.9-X}K_XMn_2O_4$ by mixing LiOH and $K_XMn_2O_4$ and heating in an annealing oven for 72 h. After preparation, the materials were characterized with X-ray diffraction and stored in argon filled dry box. Fig. 1 shows a flow chart for the preparation of the $Li_{0.9-X}K_XMn_2O_4$ material.

In addition to KOH and LiOH, the flow chart shows starting material K_2CO_3, K_2O and Li_2CO_3, Li_2O_2 and Li_2O which were used during the synthesis process. The $Li_{0.9-X}K_XMn_2O_4$ preparation also shows MnO_2 as the starting material to indicate the final product stoichiometry. Other manganese oxides (Mn_2O_3 and Mn_3O_4) were used in the process. Synthesis with the variant starting materials all yielded similar product. X-ray diffraction was used to analyze both the intermediate and final product after the heat treatment step. The heat treatment was repeated whenever incomplete conversion was indicated by the X-ray diffraction pattern.

After mixing the reactants for the potassium-doped intermediate and the final lithiated product, the materials were heated to 900 °C in air. The heat treatment involved a ∼15 min to 90% heating cycle, a 72 h soak, followed by a two-step cool

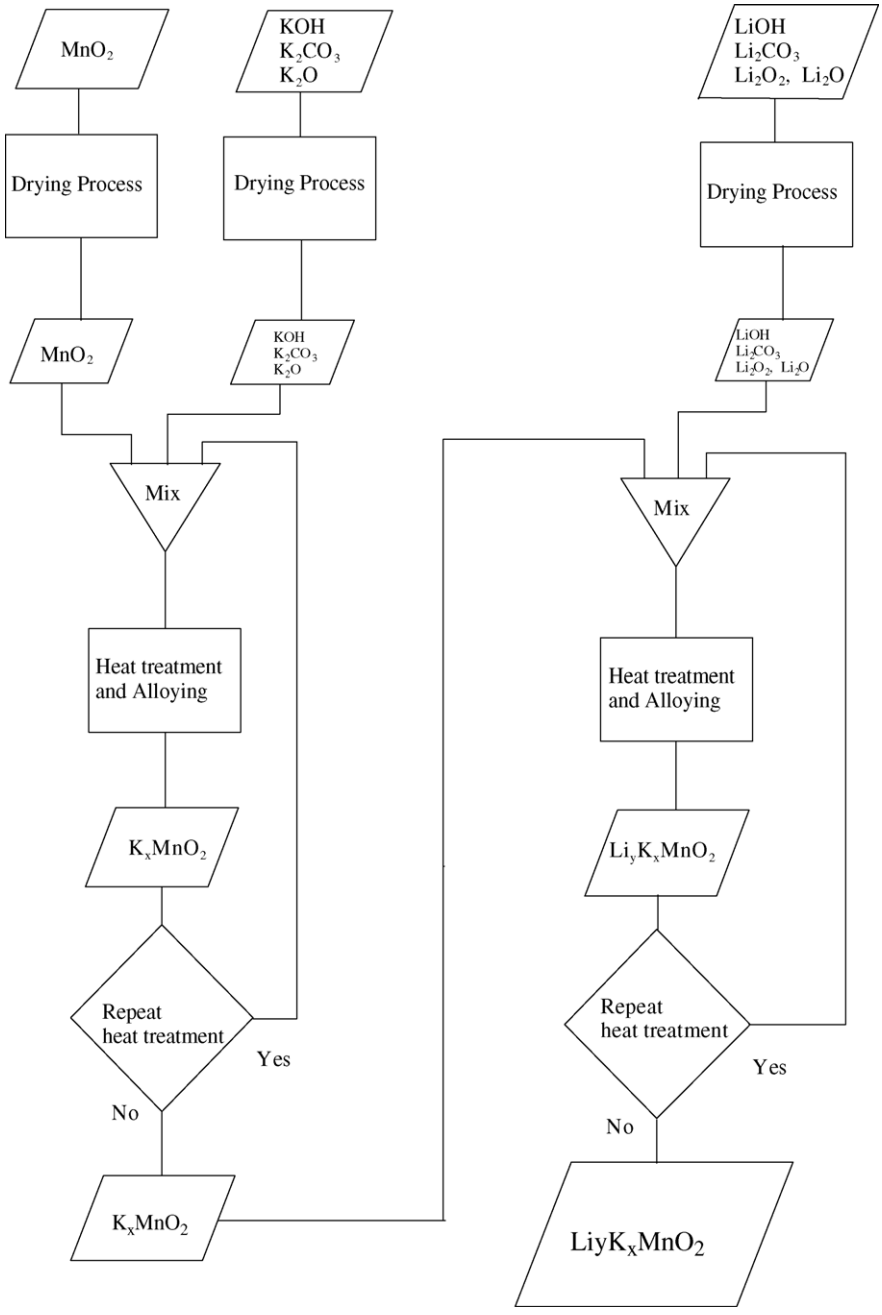

Fig. 1. Flow chart for preparation of $Li_{0.9-X}K_XMn_2O_4$ cathode material.

down of 4 h to 300 °C then quenching to 20 °C. Removing the material to ambient air performed the quenching process. Typical batch sizes were 10 g and often a second heating regiment was performed. A modified heating regiment, where the raw materials heated for 16 h at 450 °C and remixed prior to the 900 °C cycle improved the homogeneity of the product.

Initial stoichiometry included $X = 0.0$, 0.05, 0.1, 0.15, 0.2 and 0.25 in $Li_{0.9-X}K_XMn_2O_4$. Subsequent stoichiometry included $X = 0.025$, 0.075 and 0.125 in order to complete the performance matrix and 0.1, 0.15 and 0.2 stoichiometry to verify reproducibility of previous results.

Test cells were fabricated in order to evaluate the electrochemical properties of the lithium–potassium-doped manganese dioxide electrochemical system. Experimental Teflon button cells were used in the evaluation. The button cell consists of two Teflon plates with 1.9 cm diameter cylindrical recesses machined into each plate. The bottom of the recess has a small through hole for wire connection to the electrode. A nickel, stainless steel or platinum electrode current collector is set into the bottom of the recess. The sections of the test fixture are secured together with screws, this allowed for postmortem analysis of the cell components. The cell

was placed in a reaction vessel and electrolyte was backfilled into the vessel completely covering both electrodes. Additional electrochemical evaluation was conducted using conventional button cells of similar dimension of the Teflon cell.

The experimental cells were composed of a lithium anode separated from a Teflon bonded cathode with a nonwoven glass separator. The cathode was fabricated by mixing together $Li_{0.9-X}K_XMn_2O_4$, carbon and Teflon in a 6:3:1 by weight ratio, respectively. The cathode mix was rolled to 0.04 cm and dried in a vacuum oven. 0.075 cm thick lithium foil was cut using a 1.75 cm diameter (2.48 cm^2) hole punch. The cathode was also cut to 2.48 cm^2, resulting in a 0.1–0.12 g cathode. A 0.01 cm nonwoven glass separator was utilized for the separator and as a wick. The electrolyte used was 1 molar $LiPF_6$ in proportional mixtures of diethyl carbonate, dimethyl carbonate and ethylene carbonate.

The cells were cycled with an ARBIN Model BT-2043 Battery Test System. A two-step charge profile was used. The charge profile consisted of a constant current charged at 1.25 mA (0.5 mA cm^{-2}) or 2.5 mA (1 mA cm^{-2}) to 4.3 V followed by an applied constant voltage of 4.3 V. The constant voltage was maintained for 5 h or until the charge current dropped to 0.1 mA. Typically the constant voltage portion of the charge was maintained for less than 1 h before reaching the 0.1 mA cut-off current. The cells were discharged at 1.25 or 2.5 mA to 2.5 V. A rest period of 15 min between charge and discharge cycles allowed for the cells to equilibrate. The 1.25 mA profile yielded an approximately 10 h cycle time. The 2.5 mA cycle was used to speed up the cycle life study.

4. Results

Fig. 2 shows the X-ray diffraction patterns for $Li_{0.8}K_{0.2}Mn_2O_4$, $Li_{0.8}K_{0.1}Mn_2O_4$ and $Li_{0.9}Mn_2O_4$ cathode materials. Included in the figure is the 35-0782 $LiMn_2O_4$ X-ray diffraction card file. The X-ray patterns show additional diffraction angle peaks present in the potassium-doped material. It should be noted that while most of the peaks have similar magnitudes including the additional peaks there are notable exceptions. The peak at 28.5° 2Θ increases with increased potassium content and the peak at 65.5° 2Θ decreases with increasing potassium content. These X-ray patters are representative of the materials used in the cells fabricated for this paper.

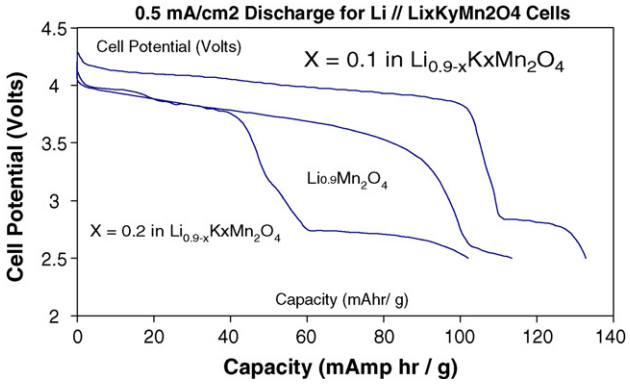

Fig. 3. Comparative discharge curves for cathode material with "*X*" in $Li_{0.9-X}K_XMn_2O_4$ equal to 0.0, 0.1 and 0.2.

Fig. 3 shows comparative discharge curves for cathode material with "*X*" in $Li_{0.9-X}K_XMn_2O_4$ equal to 0.0, 0.1 and 0.2. The data in Fig. 3 shows the 10th discharge for each cell and are typical discharges for each stochiometry. The cells for this experiment were charged and discharged at 0.5 mA cm^{-2}, which resulted in a 12–14 h discharge. The data shows the enhanced discharge capability of cells with a $Li_{0.8}K_{0.1}Mn_2O_4$ cathode. The data also shows a detrimental result for cells with a $Li_{0.7}K_{0.2}Mn_2O_4$ cathode. The data also clearly shows the two thermodynamic plateaus in

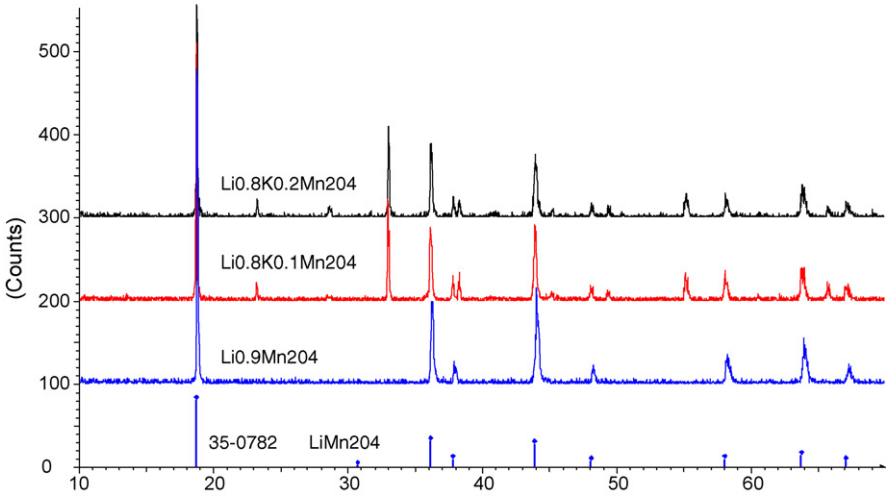

Fig. 2. X-ray diffraction patterns for $Li_{0.8}K_{0.2}Mn_2O_4$, $Li_{0.8}K_{0.1}Mn_2O_4$ and $Li_{0.9}Mn_2O_4$ cathode material.

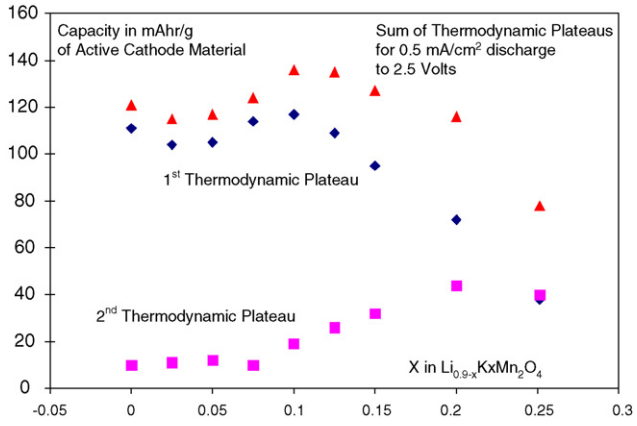

Fig. 4. Capacity obtained during discharge for $Li_{0.9-X}K_XMn_2O_4$ cathode material. Two thermodynamic plateaus (>3.0 and <3.0 V) displayed.

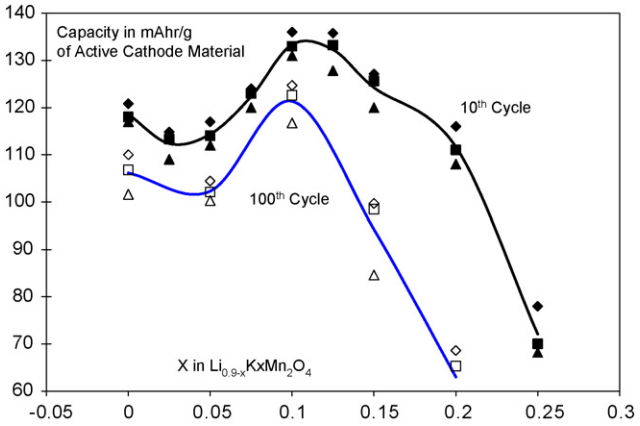

Fig. 6. Capacity delivered at the 10th and 100th cycle for $Li_{0.9-X}K_XMn_2O_4$ material.

the discharge curve indicating a phase change with lithium insertion into the cathode. Fig. 4 displays graphically the capacity obtained during discharge of the two thermodynamic plateaus. The plot shows an initial decrease in capacity delivered during the first thermodynamic plateau (>3.5 V). This initial decrease is followed by a maximum in capacity delivered as X approaches 0.1, then a steady decrease in capacity delivered as X increases greater than 0.1. The data also shows an increase in the 2.5 V plateau as X increases from 0.0 to 0.25.

Fig. 5 shows the 10th and 11th charge/discharge curve for a $Li//Li_{0.8}K_{0.1}Mn_2O_4$ cell. The cell for this experiment was charged and discharged at 0.5 mA cm^{-2} after 2 days casual storage. The data shows a coulombic over charge of 0.218 mAh for the 10th charge cycle followed by a 0.058 mAh over charge for the 11th charge. This corresponds to coulombic efficiencies of 97 and 99%. The data also shows the low over potential required for charge, resulting in a 93 and 95% energy efficient charge for the 10th and 11th cycle,

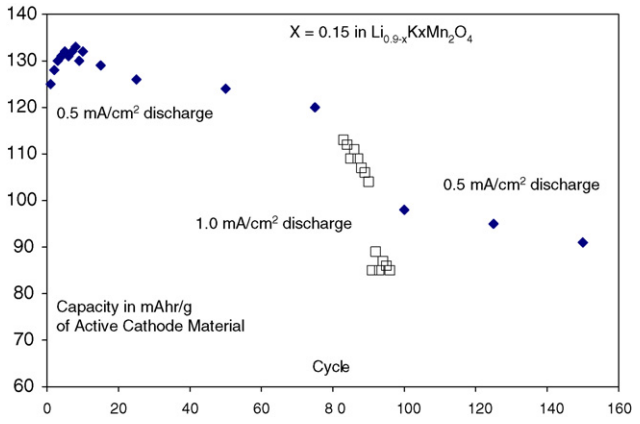

Fig. 7. Discharge data set for $Li_{0.9-X}K_XMn_2O_4$ where $X = 0.15$.

respectively. This data also clearly shows the two thermodynamic plateaus for the $Li//Li_{0.9}Mn_2O_4$ electrochemical system. Additional investigation reveals a slight two-stage division of the greater than 3.5 V thermodynamic plateau.

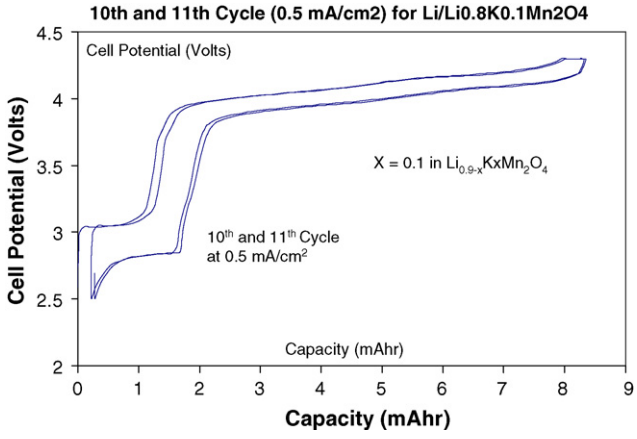

Fig. 5. Charge/discharge curve for 10th and 11th cycle for a $Li//Li_{0.8}K_{0.1}Mn_2O_4$ cell.

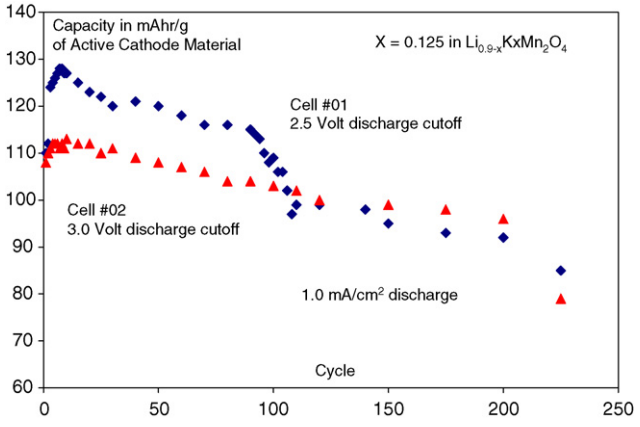

Fig. 8. Data for stoichiometry of potassium in $Li_{0.9-X}K_XMn_2O_4$ is $X = 0.125$. Cells from the same lot were discharged at 1.0 mA cm^{-2}, however, the cut-off voltage were set at 2.5 and 3.0 V.

Table 1
Performance characteristics of $Li_{0.9-X}K_XMn_2O_4$

Stoichiometry in $Li_{0.9-X}K_XMn_2O_4$	Chemical formula	Molecular weight	Theoretical capacity (mAh g^{-1}) $n = 1 - X$ ($n = 1$)	Capacity delivered to 3.0 V	Percent theoretical $n = 1 - X$ ($n = 1$)
$X = 0.0$	$Li_{0.9}Mn_2O_4$	180.12	149 (149)	111	74.6 (74.6)
$X = 0.025$	$Li_{0.875}K_{0.025}Mn_2O_4$	180.93	144 (148)	104	72.0 (70.2)
$X = 0.05$	$Li_{0.85}K_{0.05}Mn_2O_4$	181.73	140 (147)	105	74.9 (71.2)
$X = 0.075$	$Li_{0.825}K_{0.075}Mn_2O_4$	182.54	136 (147)	114	83.9 (77.6)
$X = 0.10$	$Li_{0.8}K_{0.1}Mn_2O_4$	183.34	132 (146)	117	88.9 (80.0)
$X = 0.125$	$Li_{0.775}K_{0.125}Mn_2O_4$	184.15	127 (146)	109	85.6 (74.9)
$X = 0.15$	$Li_{0.75}K_{0.15}Mn_2O_4$	184.95	123 (145)	95	77.1 (65.6)
$X = 0.20$	$Li_{0.7}K_{0.2}Mn_2O_4$	186.56	115 (144)	72	62.7 (50.1)
$X = 0.25$	$Li_{0.65}K_{0.25}Mn_2O_4$	188.17	107 (142)	38	35.6 (26.7)

Fig. 6 shows the capacity in mAh g^{-1} of active cathode material for various stoichiometry of potassium in the $Li_{0.9-X}K_XMn_2O_4$ material. The graph displays the capacity at the 10th cycle and 100th cycle. The discharge profile for this series of tests was 0.5 mA cm^{-2} through 25 cycles then 1.0 mA cm^2 charge/discharge profile for 23 cycles followed by two cycles at 0.5 mA cm^{-2}. The loss of capacity between the 75th and 100th cycle was due to the reduction and final elimination of the 2.5 V plateau. Fig. 7 shows the discharge data set for the case where the stoichiometry of potassium in $Li_{0.9-X}K_XMn_2O_4$ is $X = 0.15$. This data shows a rapid decrease in capacity during the 76th to 98th, 1.0 mA cm^{-2} cycles. Fig. 8 shows the data for the case where the stoichiometry of potassium in $Li_{0.9-X}K_XMn_2O_4$ is $X = 0.125$. Two cells from the same lot were discharged at 1.0 mA cm^{-2}, however, the cut-off voltage were set at 2.5 and 3.0 V. This test was designed to show the performance of the cell if the lower voltage plateau is not used during discharge.

5. Discussion

The data presented here shows the discharge characteristics of a family of potassium-doped lithium–manganese oxide materials. This material with the stoichiometric formula $Li_{0.9-X}K_XMn_2O_4$ where $X = 0.0$–0.25 proved to produce a viable reversible electrochemical couple with lithium. The material demonstrated a performance maximum when $X = 0.1$, where the initial specific capacity for the lithium–potassium-doped manganese dioxide electrochemical couple was 130 mAh g^{-1} of active cathode material. The discharge capacity of the system was maintained through 90 cycles (95% initial capacity). Additionally, the capacity was maintained at greater than 90% initial discharge through 200 cycles.

Table 1 compares the capacity of the synthesized potassium-doped lithium–manganese dioxide material with the stoichiometric formula $Li_{0.9-X}K_XMn_2O_4$, where $X = 0.0$–0.25 to the theoretical capacity of the material. Two values for the theoretical capacity are shown in the table: one representing a 1.0 valence change and the other $1.0 - X$ representing the stoichiometry of lithium in the reaction. A 3 V discharge termination is used since it is consistent with the application of the chemistry. Additionally a 3 V cut-off represents the sustainable capacity of the system. The capacity obtained at a 2.5 V cut-off was maintained through the initial discharges with degradation of the lower thermodynamic plateau after 90 cycles.

In addition, the data shows that synthesized potassium-doped lithium manganese oxide material with stoichiometry around the $X = 0.1$ maximum have comparable performance. These materials had an initial specific capacity in the order of 130 mAh g^{-1}, and maintained a capacity of 115 mAh g^{-1} for over 25 cycles. The capacity of the system was maintained at 90% the initial capacity through 90 cycles. After 90 cycles, a low voltage thermodynamic plateau degrades resulting in a capacity that is 75% the initial capacity. The final failure of the cell was typically due to lithium dendrites formed during charge. These dendrites form after 200 cycles and were not unexpected due to the cell design, in particular the open separator used.

References

[1] T.B. Atwater, A.J. Salkind, US Patent No. 6,770,398, 3 August 2004.
[2] D. Linden (Ed.), Handbook of Batteries, second ed., McGraw-Hill Inc., New York, NY, 1995, pp. 361–3677.
[3] J.P. Gabano, Lithium Batteries, Academic Press, New York, NY, 1983.
[4] T. Inoue, M. Sano, J. Electrochem. Soc. 145 (11) (1998) 3704–3707.
[5] Y. Xia, M. Yoshio, J. Electrochem. Soc. 144 (12) (1997) 4186–4194.
[6] D. Larcher, et al., J. Electrochem. Soc. 145 (10) (1998) 3392–3400.
[7] S.J. Wen, et al., J. Electrochem. Soc. 143 (6) (1996) L136–L138.
[8] Y. Shao-Horn, S.A. Hackney, B.C. Cornilsen, J. Electrochem. Soc. 144 (9) (1997) 3147–3153.
[9] AR. Armstrong, et al., J. Solid State Chem. 145 (1999) 549–556.
[10] X.Q. Yang, et al., Electrochem. Solid State Lett. 2 (4) (1999) 157–160.
[11] Y. Xia, M. Yoshio, J. Electrochem. Soc. 143 (3) (1996) 825–833.
[12] Y. Xia, T. Sakai, T. Fujieda, X.Q. Yang, X. Sun, Z.F. Ma, J. McBreen, M. Yoshio, Correlating capacity fading and structural changes in

$Li_{1+y}Mn_{2-y}O_{4-d}$ spinel cathode materials, J. Electrochem. Soc. 148 (July (7)) (2001) 723–729.
[13] J.B. Wachtman, Mechanical Properties of Ceramics, John Wiley & Sons, New York, NY, 1996.
[14] D.H. Jang, Y.J. Shin, S.M. Oh, J. Electrochem. Soc. 143 (9) (1996) 2204–2211.
[15] S.W. Donne, G.A. Lawrance, D.A.J. Swinkels, J. Electrochem. Soc. 144 (9) (1997) 2949–2967.